scientific reports

OPEN

Phase dependent sympathetic dysinnervation in Takotsubo syndrome revealed with transparent heart

Kiyoshi Masuyama[1], Jong-Kook Lee[2✉], Teruki Yokoyama[1], Jun Li[2], Hideki Yasutake[2], Yuki Kuramoto[1], Kyoko Hidaka[3] & Yasushi Sakata[1]

Takotsubo syndrome (TTS) is an acute cardiac syndrome characterized by transient left ventricular dysfunction. Although the wall motion abnormality resolves completely, the prognosis is poor. Defect of ^{123}I-metaiodobenzylguanidine uptake, interpreted as sympathetic impairment, persisted in TTS patients, but the mechanism is not fully understood. We aimed to elucidate morphological sympathetic nerve change in a TTS model mouse using three-dimensional imaging techniques, with a particular focus on the role of factors in these alterations. The TTS model was induced by a single intraperitoneal injection of 2.0 mg/kg adrenaline to C57BL/6 mice, resulting in transient akinesis localized to the inferior apical region of the heart. Three-dimensional morphological assessment revealed that sympathetic nerve length within the inferior apical area of TTS mice reduced during the chronic phase compared with the sham mice. Notably, the study observed a pattern of denervation during the acute phase, followed by re-innervation and subsequent denervation in the chronic phase. The neurotrophic factors expressions changed in a time-dependent manner, corresponding to the phase-specific damage both to cardiomyocytes and sympathetic neurons. The bimodal change in sympathetic nerves and altered neurotrophic factors in TTS mice provide novel insights into the pathophysiological mechanism of TTS to establish therapeutic strategies for TTS.

Keywords Cardiomyopathy, Autonomic nervous system, Pathophysiology, Basic science research

Takotsubo syndrome (TTS), a characteristic cardiac syndrome with transient left ventricular dysfunction, was first reported in 1990[1]. TTS was initially considered relatively benign because the ventricular wall motion abnormality can completely recover. However, recent studies documented that symptoms of heart failure such as breathlessness and fatigue persisted[2], and that in-hospital mortality of TTS was 4–5%, which is similar to acute coronary syndrome (ACS). Moreover, the long-term mortality associated with TTS is as poor as that of ACS[3,4]. Despite of these findings, no effective therapy has been established to improve long-term mortality in TTS patients[5].

Several molecular mechanisms have been postulated, including catecholamine-mediated myocardial stunning[5–7], disturbance in the calcium regulatory system[8,9], structural changes in cardiomyocytes[10], and acute multivessel coronary spasm[11]. However, further investigation is necessary to fully elucidate these mechanisms and develop targeted therapeutic strategies.

To further elucidate the mechanisms underlying TTS, we focused on the characteristic phenomenon of TTS, in which defects of ^{123}I-metaiodobenzylguanidine (^{123}I-MIBG) uptake persists. This persistent defect indicates impaired cardiovascular sympathetic innervation remains in the chronic phase even after the recovery of perfusion and contractility[12,13]. Previous studies have established a strong association between impaired sympathetic innervation and adverse outcomes, including increased mortality and arrhythmic events in chronic heart failure[14,15]. A significant relationship between TTS prognosis and impaired sympathetic innervation has been hypothesized, however, the specific changes of sympathetic nerves in TTS have not yet been elucidated.

[1]Departments of Cardiovascular Medicine, Graduate School of Medicine, The University of Osaka, 2-2 Yamadaoka, Suita 565-0871, Japan. [2]Departments of Cardiovascular Regenerative Medicine and Drug Discovery, Graduate School of Medicine, The University of Osaka, 2-2 Yamadaoka, Suita 565-0871, Japan. [3]Center for Fundamental Education, The University of Kitakyushu, 4-2-1 Kokura Minami-ku Kitagata, Kitakyushu 802-8577, Japan. ✉email: jlee@cardiology.med.osaka-u.ac.jp

In human studies, an elevation of catecholamine concentrations has been reported in the acute phase of TTS[6,16], and the administration of catecholamines has been shown to induce TTS[17,18]. As an elevation in the adrenaline concentration is a key factor causing TTS, previous reports have used a rodent TTS model via the injection of catecholamine[5,19–27]. We previously evaluated sympathetic nerve changes in mice with myocardial infarction (MI) using tissue clearing techniques in a three-dimensional manner[28]. These techniques enable us to evaluate morphological changes in sympathetic nerves in TTS-model mice.

In a previous in vitro study, we demonstrated that glial cell line-derived neurotrophic factor (GDNF) and nerve growth factor (NGF) promoted cardiac sympathetic innervation in a co-culture system of neonatal rat cardiomyocytes and sympathetic neurons[29]. Conversely, neural chemorepellents, such as Semaphorin-3a (Sema3a), inhibit sympathetic innervation[30]. These neurotrophic factors and neural chemorepellents might be involved in the sympathetic impairment in TTS.

In the present study, we aimed to clarify morphological changes in sympathetic nerves in TTS using three-dimensional imaging techniques and to elucidate the underlying mechanisms focusing on the involvement of neurotrophic factors.

Results
TTS mouse model
We adapted catecholamine-induced mice model. A single intraperitoneal injection of 2.0 mg/kg adrenaline was given to C57BL/6 mice. Whereas 20% of mice died within 1 week, 55% of mice (68% in survived mice) showed akinetic motion in the inferior apical area of the left ventricles within 48 h after injection (Fig. 1B and Supplemental Movies I and II), and the akinesis completely disappeared 1 week after injection. We employed these mice as the TTS model. As shown in Fig. 1A, observations were performed after 1 day, 1 week, and 4 weeks of injection, and they were defined as the acute, subacute, and chronic phases, respectively.

They were compared with sham models injected with the vehicle. There was no significant difference in baseline parameters of both models (Supplemental Table I). After injection, the TTS models showed transient akinesis in the inferior apical area of the left ventricle (Fig. 1C). There was no significant difference in baseline parameters of both models during the chronic phase (Supplemental Table II). These phenomena were similar to TTS in humans, and hence, we used these mice as TTS mice for further studies.

Sympathetic denervation in TTS mice during the chronic phase
The images of optically cleared and immunostained hearts (Fig. 2A) acquired using light sheet microscope and confocal microscope have been shown in Fig. 2B and Supplemental Movie III. Tyrosine hydroxylase (TH) is a marker for sympathetic nerves and alpha-smooth muscle actin (α-SMA) is a marker for blood vessels. Sympathetic nerves spread over the epicardial surface, similar to our previous report[28]. Then, the images of inferior basal and apical areas of sham 4w and TTS 4w mice were obtained. (Fig. 2C and Supplemental Movies IV and V).

To assess sympathetic denervation quantitatively, we tracked sympathetic nerves, measured their lengths using the Imaris software (Fig. 2D), and calculated the ratio of sympathetic nerve lengths in the inferior apical side and those in the inferior basal side. Three-dimensional analysis of the cardiac nerve showed that the ratio of nerve lengths in the inferior apical area and the inferior basal area significantly decreased in TTS chronic models (TTS 4w) compared with sham models (sham 4w vs TTS 4w, 0.92 ± 0.02 vs 0.74 ± 0.03, n = 5, p = 0.03 vs sham 4w) (Fig. 2E). Moreover, mice that did not show transient akinesis after injection of 2.0 mg/kg adrenaline did not show sympathetic denervation (Supplemental Fig. I).

In western blotting analysis, TH expression was stable in the inferior basal area but significantly decreased by 26.3% in the inferior apical area in the chronic TTS group compared with the sham group (sham 4w vs TTS 4w, n = 13, p < 0.01) (Fig. 3A, 3B and Supplemental Fig. II). These results were consistent with those from the three-dimensional imaging analysis of sympathetic nerves.

Our findings indicate that denervation occurs in the inferior apical area in the chronic phase.

Assessment of the time-course involved in denervation in TTS mice
We evaluated the time-course of denervation in TTS mice by investigating the acute (1 day), subacute (1 week), and chronic (4 weeks) phases (Fig. 4A). The ratio of nerve lengths in the inferior apical area and the inferior basal area was significantly decreased in the acute phase (sham 1d vs TTS 1d, 1.09 ± 0.02 vs 0.82 ± 0.03, n = 4, 5 respectively, p = 0.02) (Fig. 4B). After denervation in the acute phase, the ratio of nerve length was significantly increased during the subacute phase (TTS 1d vs TTS 1w, 0.82 ± 0.03 vs 1.18 ± 0.03, n = 5, p < 0.01) (Fig. 4C). In contrast, denervation occurred again in the chronic phase (TTS 1w vs TTS 4w, 1.18 ± 0.03 vs 0.74 ± 0.03, n = 5, p < 0.01) (Fig. 4C and Supplemental Fig. III).

Alteration in the gene expressions in TTS mice
We examined the gene expression of *Ngf*, *Gdnf*, and *Sema3a* in the inferior basal and inferior apical areas to elucidate how neurotrophic factors changed in a phase-dependent manner.

During the acute phase, *Gdnf* expression in the inferior basal and inferior apical areas increased in the TTS by 8.37- and 7.46-folds respectively compared with the sham models (sham 1d vs TTS 1d, n = 9, p < 0.01) (Fig. 5A). In contrast, no significant difference was observed in *Ngf* expression (Fig. 5B). During the subacute phase, *Gdnf* expression in the inferior basal area increased in the TTS by 1.60-folds compared with the sham models (sham 1w vs TTS 1w, n = 6, 5 respectively, p = 0.02) (Fig. 5A). *Ngf* expression in the inferior apical area decreased by 28.9% in the TTS compared with the sham models (sham 1w vs TTS 1w, n = 6, 5 respectively, p = 0.02) (Fig. 5B). During the chronic phase, no significant difference was observed in the expression of *Gdnf* and *Ngf* between the TTS and sham models (Fig. 5A,B and Supplemental Figure IVA,B).
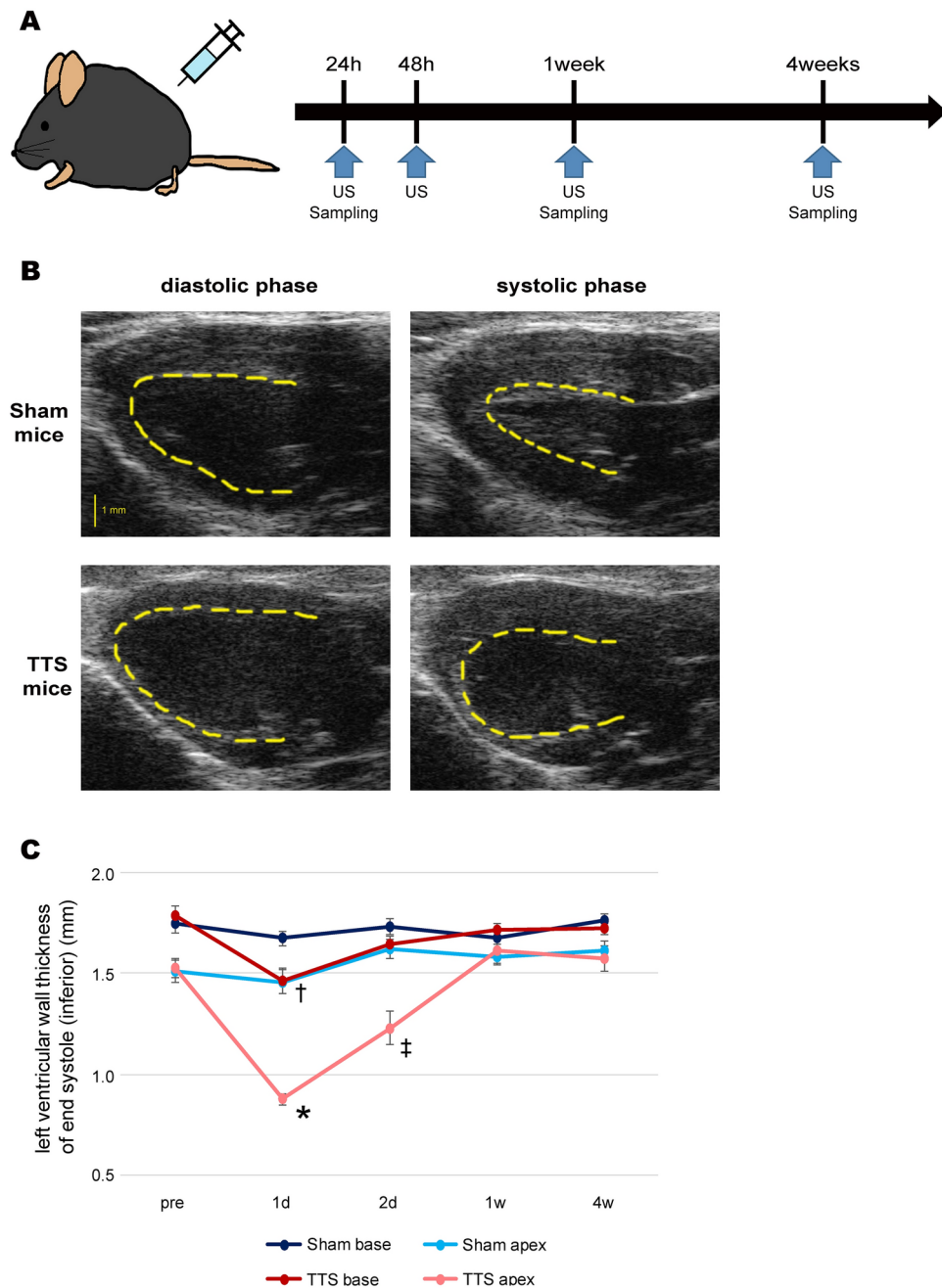
Fig. 1. Establishment of Takotsubo syndrome (TTS) mouse model. (**A**) Experimental protocol for the establishment of TTS models. Mice received intraperitoneal injection of adrenaline and mice were examined by echocardiography at 24 h (1 day)/48 h (2 days)/1 week/4 weeks after injection. Sham mice were injected with the vehicle. Sampling was performed at 1 day/1 week/4 weeks after injection. (**B**) Echocardiography of Sham and TTS mice. Left panels indicate the diastolic phase and right panels indicate the systolic phase. The endocardial side is traced by yellow dashed lines. Scale bar, 1 mm. (**C**) Left ventricular wall thickness at the end systolic phase of the inferior base of Sham mice (blue), the inferior apex of Sham mice (light blue), the inferior base of TTS mice (red), and the inferior apex of TTS mice (pink) were measured at pre-injection and 1 day/2 days/1 week/4 weeks after injection (n = 19 and, 16 respectively). Statistical significance was determined using the Mann–Whitney U-test. †P < 0.01, Sham base at 1 day, *P < 0.01, vs. Sham apex at 1 day, ‡P < 0.01, vs. Sham apex at 2 days. Error bars represent standard error of the mean.

Sema3a expression increased in both the areas by 1.65- and 1.52-folds respectively during the acute phase (sham 1d vs TTS 1d, n = 9, p < 0.01) and decreased by 40.7% in the inferior apical area during the chronic phase (sham 4w vs TTS 4w, n = 4, p = 0.03) (Fig. 6 and Supplemental Fig. IVC).

We next investigated the state of the neurons, focusing on changes in the gene expression of NGF receptors, including neurotrophic tyrosine kinase receptor type1(Ntrk-1) and nerve growth factor receptor (Ngfr)
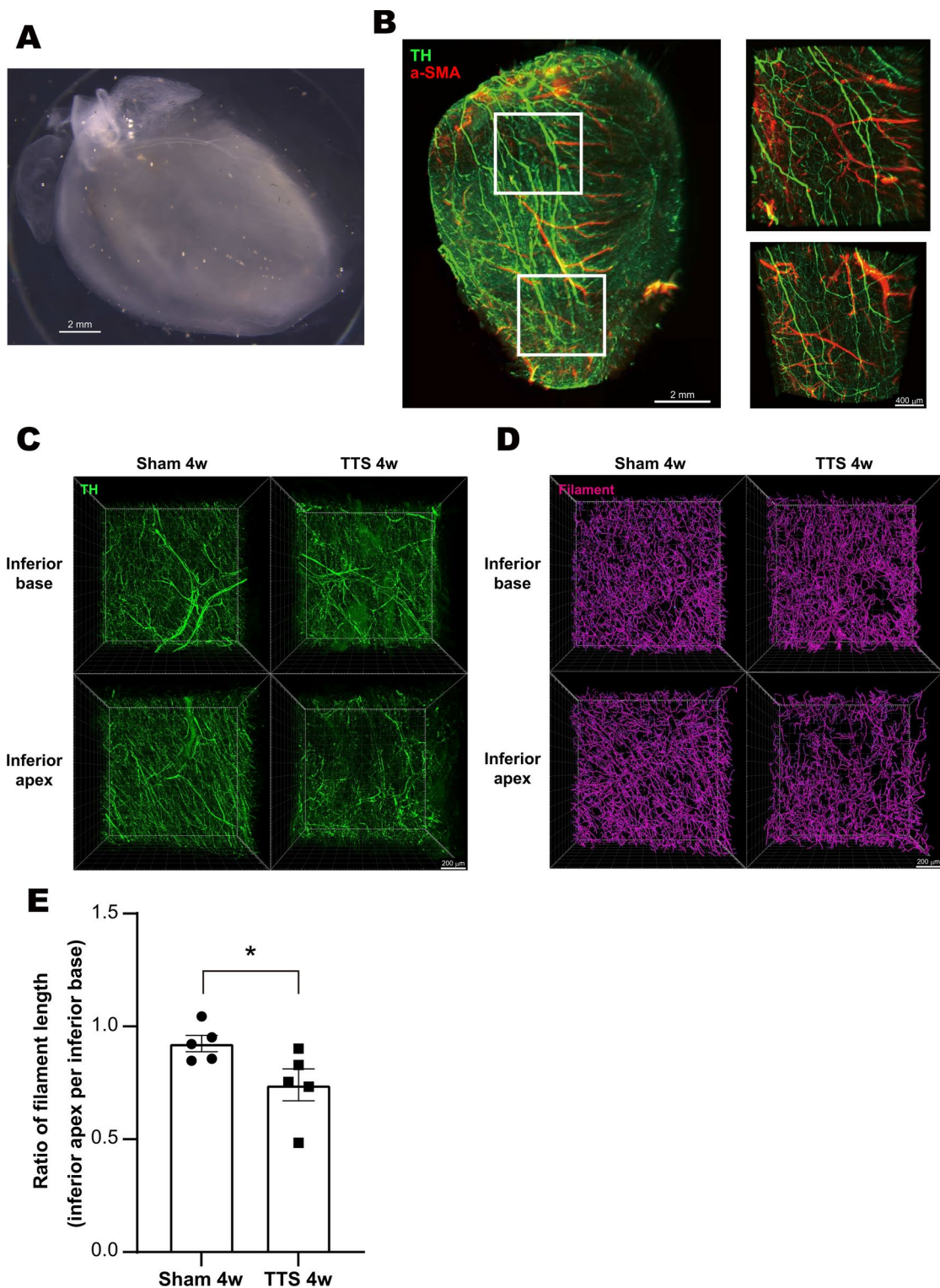
(Supplemental Fig. V). *Ntrk-1* expression increased in both areas during the acute phase and decreased in both the areas during the chronic phase. In contrast, *Ngfr* expression did not show significant differences during any phase. Additionally, we assessed the mechanical stress in the regions by measuring natriuretic peptide B(Nppb) expression (Supplemental Fig. VI). During the acute phase, *Nppb* gene expression was upregulated in both areas, with a higher degree of the upregulation observed in the inferior apical area.

Discussion

In this study, we successfully visualized sympathetic denervation in TTS mice in the chronic phase and demonstrated dynamic changes in the sympathetic nerve structure along with phase-dependent alterations in neurotrophic factor expressions for the first time.

◄**Fig. 2**. Three-dimensional distribution of sympathetic nerve in the heart of Takotsubo syndrome (TTS) mice. (**A**) Bright field image of murine heart after CUBIC procedure. Scale bar, 2 mm. (**B**) Three-dimensional images of tyrosine hydroxylase (TH) (green)-stained and α-smooth muscle actin (α -SMA) (red)-stained heart samples observed using light sheet microscope (Lightsheet Z.1, Carl Zeiss). TH represents sympathetic nerves, and α -SMA is a marker of blood vessels. Scale bar, 2 mm. The right figures show higher magnified views of the boxed region in the left figure. Scale bar, 400 μm. (**C**) Three-dimensional images of the heart obtained from 4-week Sham and 4-week TTS mice. Heart samples were immunostained for TH (green). Sympathetic nerves in the inferior basal area and the inferior apical area were observed by confocal microscope (LSM700, Carl Zeiss). Scale bar, 200 μm. (**D**) Filament analysis of the sympathetic nerves (magenta) in 4-week Sham and 4-week TTS mice using the Imaris software. Scale bar, 200 μm. (**E**) Quantitative analysis of the sympathetic nerves. The ratio of the sympathetic nerve length in the inferior apical area to that in the inferior basal was statistically analyzed between 4-week Sham and 4-week TTS mice (n = 5 each). Statistical significance was determined using the Mann–Whitney U-test. *P < 0.05, vs. 4-week Sham mice. Error bars represent standard error of the mean.
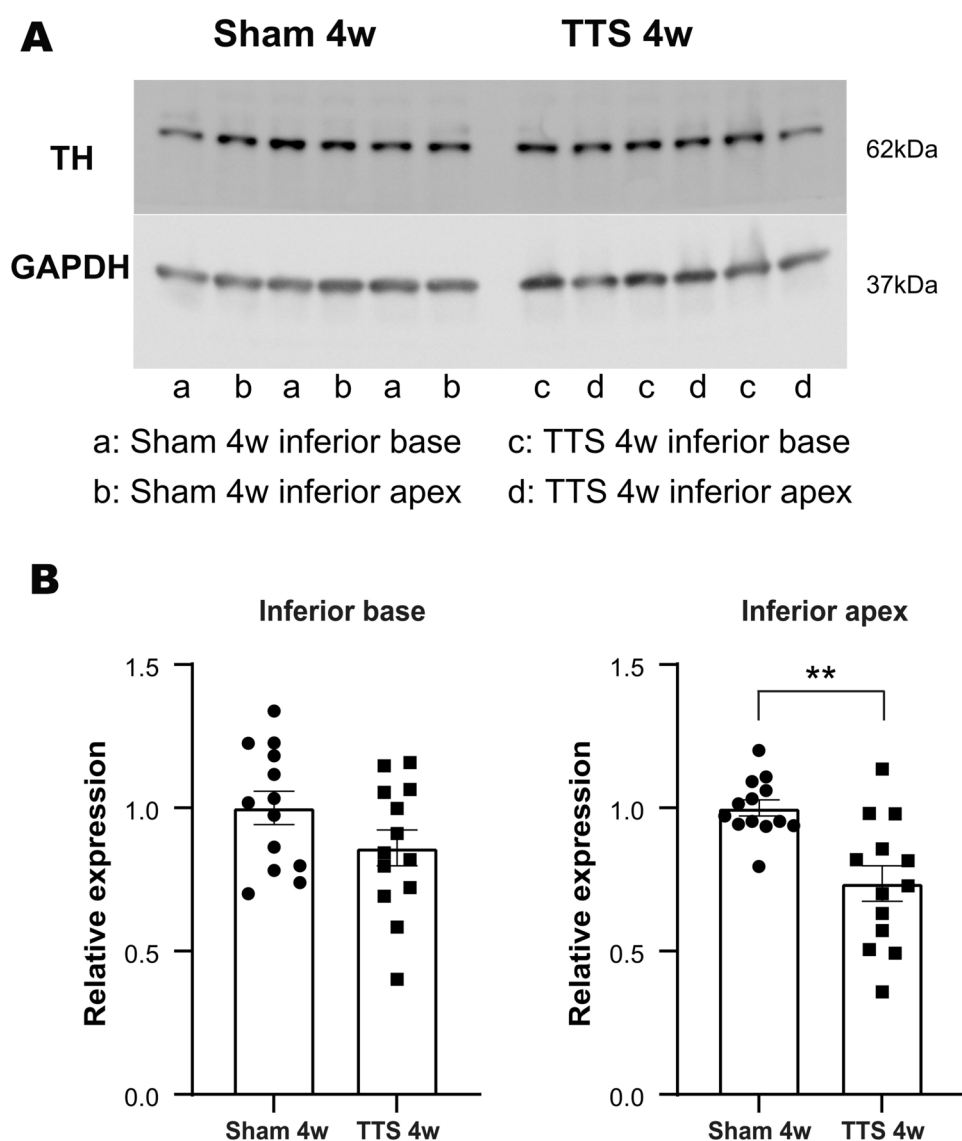

Fig. 3. Protein expression of tyrosine hydroxylase in 4-week Sham and 4-week Takotsubo syndrome (TTS) mice. (**A**) Total protein was extracted from the inferior basal and the inferior apical area of 4-week Sham and 4-week TTS mice, and tyrosine hydroxylase (TH) expression was analyzed by western blotting. (**B**) TH expression was quantified by densitometry. GAPDH was used as an internal control for total proteins (n = 13 each). Statistical significance was determined using the Mann–Whitney U-test. *P < 0.01, vs. 4-week Sham mice. Error bars represent standard error of the mean.
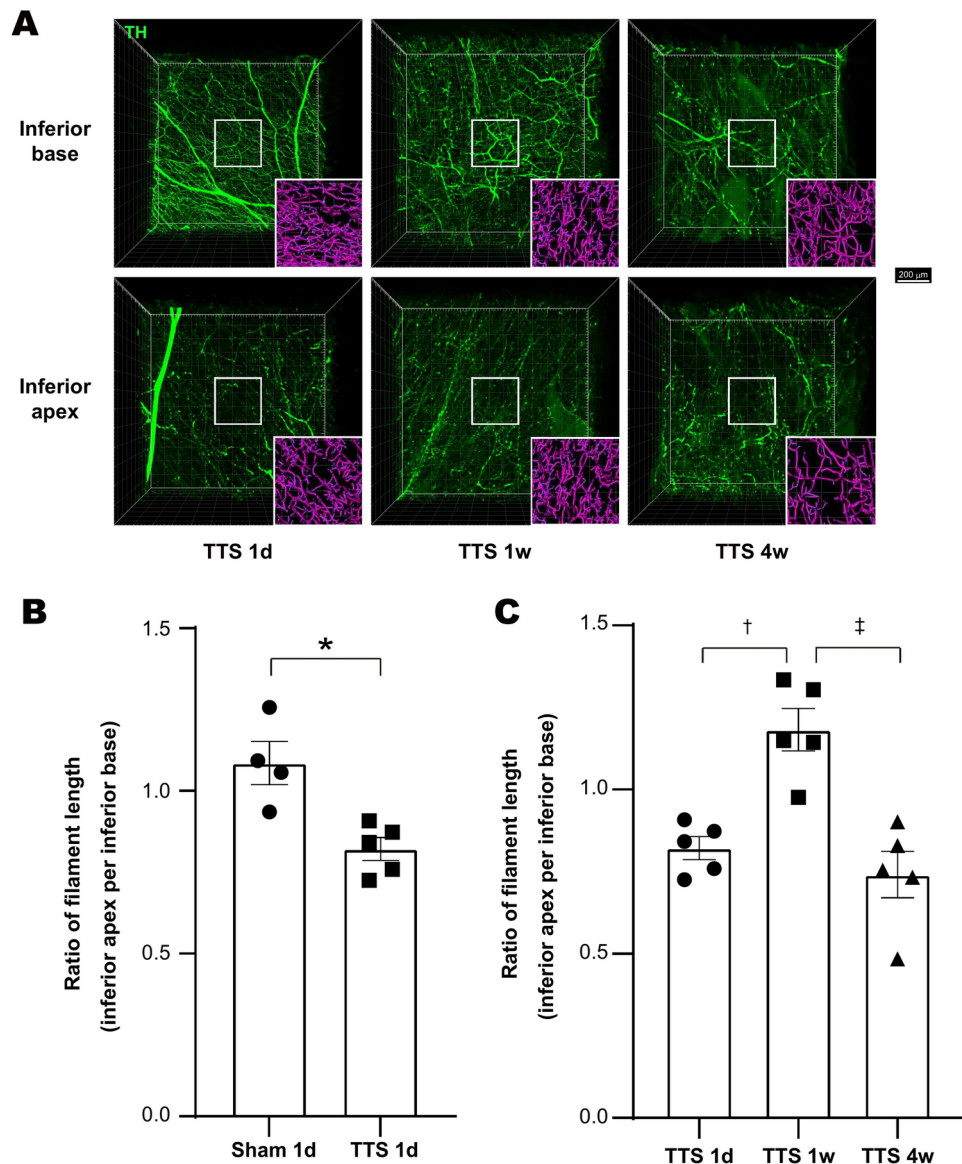
Fig. 4. Three-dimensional image of sympathetic nerve distribution in the acute, subacute, and chronic phase of Takotsubo syndrome (TTS) mice. (**A**) Three-dimensional image of sympathetic nerve (green) at the inferior basal and the inferior apical area in TTS mice at the acute (TTS 1d), subacute (TTS 1w), and chronic (TTS 4w) phases. The lower right panels are magnified and tracked with a filament analysis view of the boxed region of each image. Scale bar, 200 μm. (**B**) Quantitative analysis of the sympathetic nerves. The ratio of the sympathetic nerve length in the inferior apex to that in the inferior base was statistically analyzed between 1-day Sham and TTS mice (n = 4, 5 respectively). Statistical significance was determined using the Mann–Whitney U-test. *P < 0.05, vs. 1-day Sham mice. Error bars represent standard error of the mean. (**C**) Analysis of sympathetic nerves in TTS mice over time. The ratio of filament length between the inferior apex and the inferior base in TTS in each phase (n = 5). Statistical significance was determined by one-way analysis of variance followed by the Turkey's multiple comparisons test. †P < 0.01, vs. 1-week TTS mice. Error bars represent standard error of the mean.

Animal model and the limitation of the study

TTS predominantly affects females. Some studies using ovariectomy models[22,31,32] have shown that estrogen plays a protective role in TTS and other heart disease. However, these models cannot completely avoid the effect of surgery. To investigate the precise mechanism, we used male mice, which are not influenced by surgery and estrogen.

This model is based on exogenous adrenaline administration. It may differ from endogenous adrenaline overproduction model.
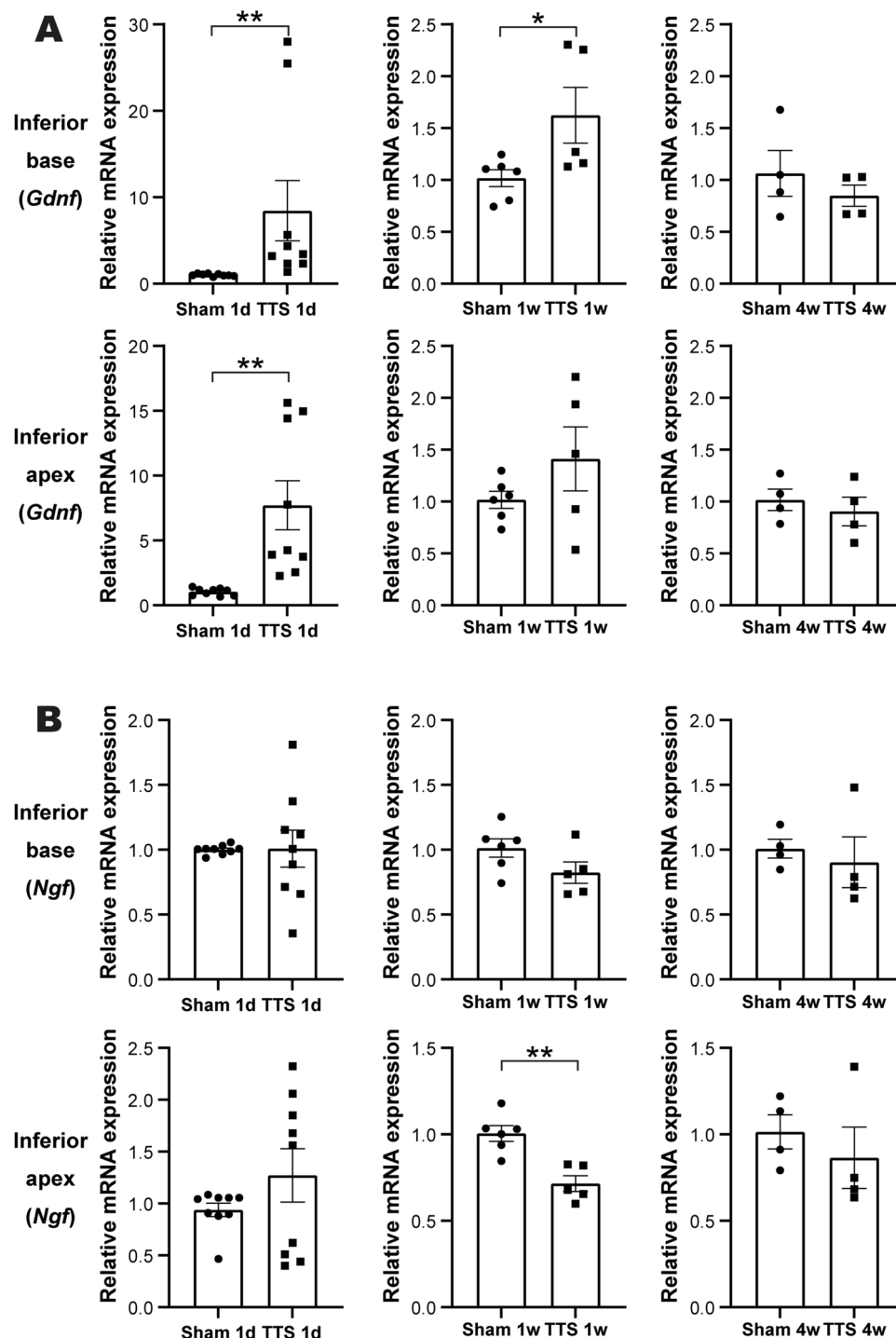
Fig. 5. Gene expression of neurotrophic factors. (**A,B**). The expression of *Gdnf* (**A**) and *Ngf* (**B**) in the inferior base and the inferior apex from Sham mice and Takotsubo syndrome mice were analyzed by quantitative reverse transcription polymerase chain reaction (n = 9, 9, 6, 5, 4, and 4, respectively). Statistical significance was determined using the Mann–Whitney U test. *P < 0.05 vs. Sham mice, **P < 0.01 vs. Sham mice. Error bars represent standard error of the mean.

Implications of persistent sympathetic dysfunction in TTS

We first visualized the three-dimensional structure of the cardiac sympathetic neural network in TTS mice and demonstrated that sympathetic denervation occurred mice in the chronic phase. The observed defects in ^{123}I-MIBG uptake in patients with TTS could be partially explained by sympathetic denervation. Additionally, long-lasting symptoms of heart failure such as breathlessness and fatigue are developed in the chronic phase[2], suggests existence of persistent damage in the chronic phase of TTS. Our findings indicate that sympathetic
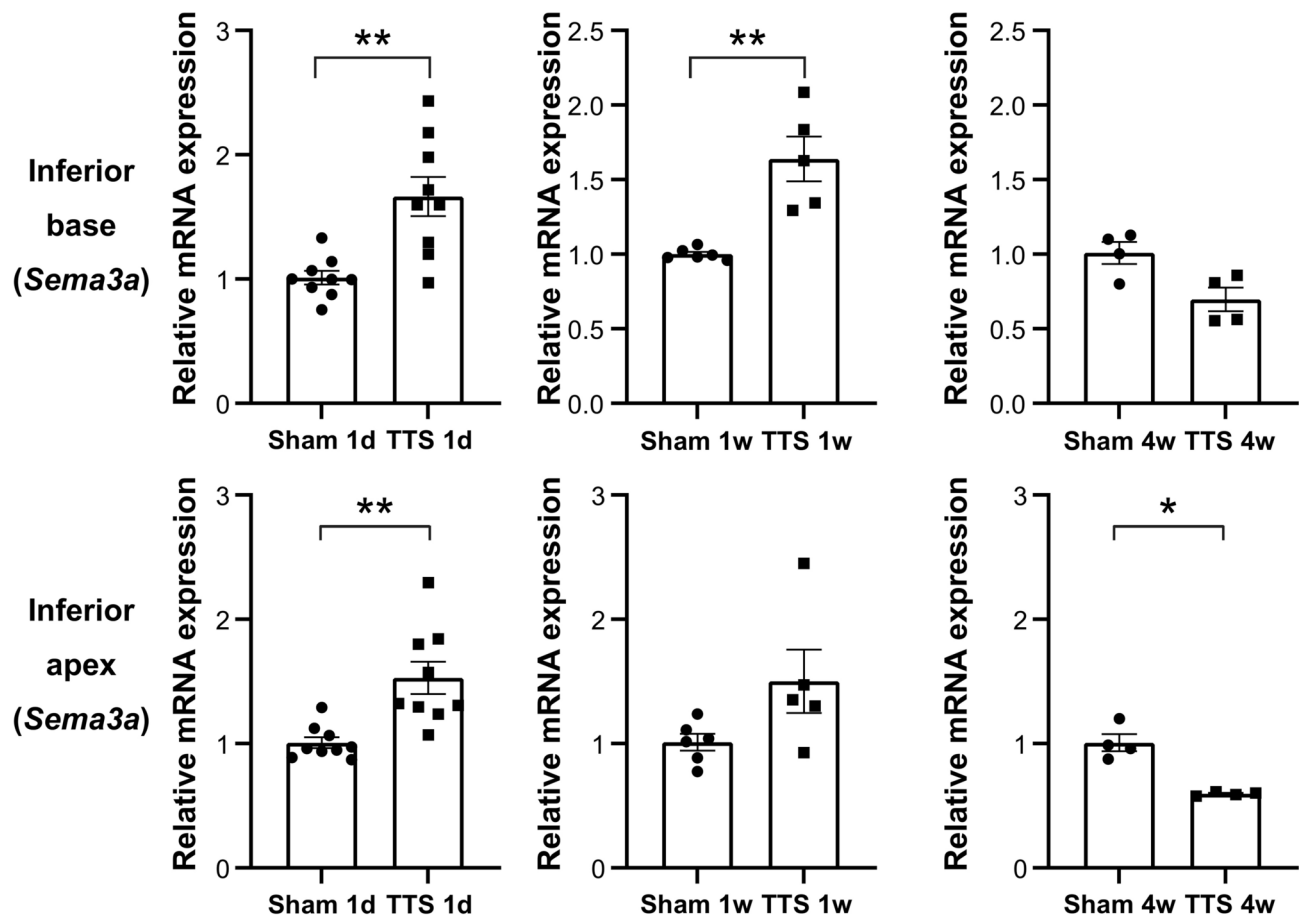
Fig. 6. Gene expression of *Sema3a*. The expression of *Sema3a* in the inferior base and the inferior apex of Sham and Takotsubo syndrome mice were analyzed by quantitative reverse transcription polymerase chain reaction (n = 9, 9, 6, 5, 4, and 4, respectively). Statistical significance was determined using the Mann–Whitney U test. *P < 0.05 vs. Sham mice, **P < 0.01 vs. Sham mice. Error bars represent standard error of the mean.

denervation contributes to these chronic symptoms, highlighting the importance of addressing sympathetic dysfunction in TTS management.

Transient dysinnervation underlies the pathophysiology of TTS

We also investigated the progression of denervation during the chronic phase of TTS. Remarkably, the sympathetic nerve length exhibited a bimodal course (Fig. 4), with denervation occurring initially during the acute phase, followed by re-innervation during the subacute phase, and subsequent denervation occurred again in the chronic phase. This contrasts with reports that defects in ^{123}I-MIBG persist throughout the course of TTS[13,33]. This discrepancy suggests that different mechanisms may be responsible for the defects in ^{123}I-MIBG uptake in each stage of the disease.

Previous reports have mentioned about mechanisms[34]: for example, diminished sympathetic nerves, competition with excessive adrenaline, downregulation of β-adrenergic receptors, and decrease in adrenaline re-uptake. However, the precise mechanisms underlying the persistent ^{123}I-MIBG defects observed in TTS mice remain to be fully elucidated.

In the acute phase, our study revealed that sympathetic nerves diminished, which suggested that sympathetic denervation contributes to defect of ^{123}I-MIBG uptake in this phase.

During the subacute phase, we observed re-innervation was observed, indicating that the ^{123}I-MIBG defect was caused by a different mechanism other than sympathetic denervation. Previous research on a monocrotaline-induced pulmonary hypertension rat model showed that ^{123}I-MIBG defects caused by re-uptake dysfunction with sympathetic hyper-innervation[35]. In the present study, we hypothesized that the biophysical stimuli caused by the akinetic inferior apical area may contribute to re-innervation, while the re-uptake function was impaired.

In the chronic phase, denervation occurred again, which indicated that the defect of ^{123}I-MIBG uptake at this stage reflects diminished sympathetic innervation. Consistent with our results, a previous study reported evidence of sympathetic fiber loss in a chronic heart failure model[36]. Notably, although our TTS model showed the recovery of contractility, the animals presented a similar phenotype of sympathetic denervation as with the chronic heart failure model, underscoring the potential long-term impact of TTS on sympathetic innervation.

Based on the observations across the acute, subacute, and chronic phases, transient sympathetic dysinnervation appears to underlie the pathophysiology of TTS and could be a candidate for therapeutic intervention. A similar pattern of bimodal change in the sympathetic nerves has been reported in the progression from cardiac hypertrophy to heart failure[37].

Underlying mechanisms of transient dysinnervation

NGF and GDNF have been reported to promote sympathetic innervation[29,38–40], whereas Sema3a inhibits innervation[41]. Our results suggested that damage to not only cardiomyocytes but also neuronal cells contribute to the transient dysinnervation, although functional analyses were not performed in the study.

In the acute phase, the upregulation of *Gdnf* and *Ntrk-1* gene expression observed in both the inferior basal and the inferior apical area during the acute phase was considered a result of denervation. The findings on the *Nppb* gene expressions imply that localized akinesis in the inferior apical area induced greater mechanical stress compared to the inferior base area, leading to sympathetic denervation. This is supported by previous reports showing that mechanical stress causes myelin protein loss and diffuse axonal injury[42,43]. Additionally, adrenaline has been shown to induce time- and concentration-dependent loss of viability in neuronal cells[44] and chronic unpredictable mild stress promotes neuronal apoptosis in the cerebral cortex[45]. Taken together, the mechanisms of denervation during the acute phase involve neuronal damage due to excessive stretch caused by localized akinesis, neuronal direct damage, and cardiomyocyte damage.

In the subacute phase, the increased expression of *Ntrk-1* and *Ngfr* might have induced re-innervation, while the decreased expression of *Ngf* during this phase might have contribute to sympathetic denervation in the chronic phase. The sympathetic denervation in TTS could be caused by downregulation of NGF, that was similar to the mechanisms reported in a chronic heart failure model[36].

In the chronic phase, *Ngf* expression recovered, whereas *Sema3a* expression decreased, thereby promoting innervation. Since cardiomyocytes modulate NGF and Sema3a levels[39,46], cardiomyocyte function of sympathetic innervation was restored in the chronic phase. The downregulation of *Ntrk-1* gene expression during the chronic phase confirms sympathetic neural damage in this phase. We speculate that the persistent sympathetic denervation is primarily due to sympathetic neural damage.

Taken together, the transient sympathetic dysinnervation is the result from combined damage to both sympathetic nerves and cardiomyocytes.

Prognosis and therapeutic targets to TTS

TTS had been considered as a benign disease, but recent studies revealed that the prognosis of TTS was poor and comparable to MI[3,4]. The persistent defect of ^{123}I-MIBG uptake is a characteristic phenomenon of TTS[12,13] and similar defects have been correlated with arrhythmia and cardiac death in MI[47–49]. From these reports, impaired sympathetic innervation plays a pivotal role in cardiovascular diseases and is closely associated with poor prognosis.

We observed sympathetic denervation in TTS mice, a phenomenon that has also been reported in MI[28]. Heterogeneous electrophysiological changes in the denervated area make the heart more vulnerable to lethal ventricular arrhythmias[50].

Sympathetic denervation is also thought to contribute to arrhythmogenicity and poor prognosis in TTS. Strategies have not been established to improve prognosis for TTS patients; therefore, interventions based on sympathetic denervation could comprise a novel therapeutic strategy. This study is the first to report morphological transition in sympathetic nerves in TTS mice. We also evaluated the neurotrophic factors underlying the dynamic alterations in sympathetic nerves in TTS mice. Our findings indicate that sympathetic denervation involves both cardiomyocyte and sympathetic neural damage, and targeting this sympathetic denervation could be a novel therapeutic strategy to improve outcomes in TTS patients.

Methods

Animals and experimental protocols

All animal procedures were performed in accordance with the National Institutes of Health guidelines (Guide for the Care and Use of Laboratory Animals). All experiments were approved by Committee of the University of Osaka (approval number: 28–028-010) and performed in conformity with ARRIVE guidelines. Wild type mice (C57BL/6 J) were obtained from Charles River Laboratories Japan Inc. (Yokohama, Japan). The animals were fed ad libitum with standard rodent chow and water under conditions of ambient temperature (23 ± 1.5 °C) and a 12-h light/dark cycle in institution-specific pathogen-free housing with care. For tissue collection, mice were euthanized by bilateral pneumothorax after intraperitoneal injection of 0.4 ml 20% Urethane.

The 3-month-old male mice weighing 25–30 g received a single intraperitoneal injection of 2.0 mg/kg of adrenaline. Vehicle-injected age-matched mice were used as sham mice. Cardiac function was evaluated by echocardiography before the injection and at 24 h, 48 h, 1 week, and 4 weeks after the injection (Fig. 1A). Transthoracic echocardiography was performed using the Vevo 770 imaging system (Visualsonics, Inc., Toronto, Canada). M-mode echocardiographic images of longitudinal view were obtained to measure the size and function of left ventricle (LV). Wall thickness of the inferior basal and inferior apical area at the end systole was evaluated to identify regional differences. We used mice that showed transient akinesis in the inferior apical area as TTS mice.

For baseline characteristics, we measured body weight (BW), heart rate (HR), LV end-diastolic diameter (LVDd), LV end-systolic diameter (LVDs), and fractional shortening (FS). In 4 weeks after injection, in addition to these parameters, heart weight (HW) and heart-to-body weight ratio (HW/BW) of sham and TTS models were measured.

Western blotting

Heart tissue was divided into four sections to evaluate regionality in detail, and then homogenized and lysed with radioimmunoprecipitation assay buffer containing protease and phosphatase inhibitor cocktails for 30 min on ice. Lysates were centrifuged at 15,000 g for 20 min, and the supernatants were used as the whole-cell extracts. The protein samples were separated by SDS-PAGE and transferred onto nitrocellulose membranes (GE Healthcare, Boston, MA, USA). The membranes were incubated with primary antibodies, followed by horseradish peroxidase-conjugated anti-rabbit and anti-goat IgG (Jackson ImmunoResearch, West Grove, PA, USA). Immunoreactive signals were detected using ECL Plus Western Blotting Detection System (GE Healthcare). The following primary antibodies were used for western blotting: anti-tyrosine hydroxylase (TH) antibody (rabbit polyclonal 1: 1000, AB152, Merck KGaA, Darmstadt, Germany) and anti-GAPDH antibody (rabbit monoclonal 1: 10,000, #2118, Cell Signaling Technology, Danvers, MA, USA).

RNA analysis

Total RNA was extracted using the PureLink RNA Mini Kit (Ambion, Thermo Fisher Scientific, Waltham, MA, USA) for heart tissues according to the manufacturer's instructions. RNA samples were reverse-transcribed using the SuperScript VILO cDNA Synthesis Kit (Invitrogen, Thermo Fisher Scientific). Quantitative real-time polymerase chain reaction was performed using the Universal Probe Library (UPL, Roche, Basel, Switzerland) and THUNDERBIRD Probe qPCR Mix (TOYOBO, Osaka, Japan) using LightCycler 480 (Roche). Relative expression of target genes was normalized using the expression of the internal control gene by the comparative Ct method. Primer sequences and corresponding UPL numbers were designed using the online program provided by Roche. The following primers and probes were used in this study: *Gapdh* #52, 5′-GGGTTCCTATAAATAC GGACTGC-3′; and 5′-CCATTTTGTCTACGGGACGA-3′; *Gdnf* #70, 5′-TCCAACTGGGGGTCTACG-3′; and 5′-GACATCCCATAACTTCATCTTAGAGTC-3′; *Ngf* #10, 5′-GTGCCTCAAGCCAGTGAAA-3′; and 5′-GAC CACAGGCCAAAACTCC-3′; *Sema3a* #72, 5′-ATCAGTGGGTGCCTTACCAA-3′; and 5′-TCCGCCAAATGT TTTACTGG-3′; *Ntrk-1* #20, 5′-TGTCCAAGTCAGCGTCTCC-3′; and 5′-AAGGGGATGCACCAATGAT-3′; *Ngfr* #26, 5′-ACTGAGCGCCAGTTACGC-3′ and 5′-CGTAGACCTTGTGATCCATCG-3′; *Nppb* #71, 5′-GTC AGTCGTTTGGGCTGTAAC-3′; and 5′-AGACCCAGGCAGAGTCAGAA-3′.

Reagents and solutions

Paraformaldehyde (PFA) (162–1665), urea (219–00,175), and 2,2',2"-nitrilotriethanol (145–05,605) were purchased from Wako Pure Chemical Industries, Ltd. (Osaka, Japan). Polyethylene glycol mono-p-isooctylphenyl ether (Triton X-100) (35,501–15) was purchased from Nacalai Tesque (Kyoto, Japan). N,N,N',N'-tetrakis (2-hydroxypropyl) ethylenediamine (T0781) was purchased from Tokyo Chemical Industry Co. Ltd. (Tokyo, Japan). The CUBIC-1 reagent was prepared by mixing 25% urea, 25% N,N,N',N'-tetrakis (2-hydroxypropyl) ethylenediamine, and 15% Triton X-100 in deionized water. The CUBIC-2 reagent was prepared by mixing 50% sucrose, 25% urea, 10% 2,2',2"-nitrilotriethanol, and 0.1% (v/v) Triton X-100 in deionized water. Both the CUBIC reagents were freshly prepared and degassed before use.

Heart tissue clearing and fluorescence labeling

Tissue clearing of the heart was performed according to the CUBIC-perfusion protocol reported by Tainaka et al[51,52]. For transcardial perfusion, a 21-gauge needle was inserted into the left ventricle through the apex. Mice were transcardially perfused with 10 mL of cold phosphate-buffered saline (PBS) containing 10 U/mL of heparin to remove the blood, 150 mL of cold 4% (w/v) PFA in PBS, 20 mL of PBS to wash out PFA, and 20 mL of 50% (v/v) CUBIC-1 reagent (1:1 mixture of PBS: CUBIC-1). Hearts were excised and continuously immersed in 30 mL of CUBIC-1 reagent at 37 °C for 2 weeks with gentle shaking. The fresh reagent was exchanged every day in the first week and every other day in the second week. After treatment with CUBIC-1 reagent, the hearts were washed with PBS three times for 30 min at room temperature with gentle shaking, immersed in 20% (w/v) sucrose in PBS at room temperature, and then frozen in OCT compound (Sakura Finetek, Tokyo, Japan) at − 80 °C overnight. The next day, the frozen samples were thawed, washed with PBS three times for 30 min (each), and subjected to immunostaining with anti-TH antibody (rabbit polyclonal 1:200, AB152, Chemicon, Temecula, CA, USA) in 0.1% (v/v) Triton X-100, 0.5% (w/v) bovine serum albumin (BSA), and 0.01% sodium azide in PBS for 5 days at 37 °C with gentle shaking. The stained samples were then washed with 10 mL of 0.1% Triton X-100 in PBS (PBST) three times for 30 min (each) at 37 °C with gentle shaking and stained with Cy3-conjugated anti-actin α−smooth muscle antibody (mouse monoclonal 1:200, C6198, GE Healthcare) and fluorescence-conjugated secondary antibodies: Alexa Fluor 647-conjugated donkey anti-rabbit IgG (1:200, Invitrogen) in 0.1% (v/v) Triton X-100, 0.1% (w/v) BSA, and 0.01% (v/v) sodium azide in PBS for 5 days at 37 °C with gentle shaking. The stained samples were then washed with 30 mL of PBST at 37 °C with gentle shaking three times for 30 min (each), immersed in 20% (w/v) sucrose in PBS, and degassed and immersed in CUBIC-2 reagent with gentle shaking at 37 °C overnight. The next day, CUBIC-2 reagent was changed, and the samples were further incubated for three days.

Image acquisition and image processing

Images of CUBIC-cleared and immunofluorescently labeled heart tissues were acquired using the light sheet microscope light sheet Z.1 (Carl Zeiss, Jena, Germany) equipped with a 5×objective lens (EC Plan-Neofluar 5×, numerical aperture (NA) = 0.16, working distance (WD) = 18.5 mm) and LSM 700 confocal microscope (Carl Zeiss) equipped with a 10×objective lens (EC Plan-Neofluar 10×, NA = 0.3, WD = 5.2 mm). Heart tissue samples were immersed in CUBIC-2 reagent during image acquisition. Three-dimensional reconstruction of Z-stacks and conversion to movies were performed using the Zen (Carl Zeiss) or Imaris software (Bitplane, Zurich, Switzerland).

Quantification of cardiac sympathetic innervation

TH immunostaining was performed to evaluate the length of cardiac sympathetic nerves. The three-dimensional images of cardiac sympathetic nerves, obtained by confocal microscope, were used to perform innervation analyses.

The inferior basal area and inferior apical area were selected (1280.35 μm × 1280.35 μm) for each sample, and nerve length was measured using a computer-assisted image analysis system (Measurement Pro application of Imaris software, Bitplane).

Statistical analysis

All statistical analyses were performed using EZR[53], a modified version of R commander designed to add statistical functions frequently used in biostatistics. Data are expressed as mean ± standard error of the mean. Groups were compared and the significance of the differences between two groups was determined by the Mann–Whitney U-test, whereas that among three groups was analyzed by one-way analysis of variance and the Tukey's multiple comparisons test. In addition, the significance of the differences among the samples was determined using Wilcoxon matched-pairs signed rank test. A p-value of < 0.05 was considered statistically significant. Graphs were prepared using GraphPad Prism (GraphPad Software Inc., La Jolla, CA, USA).

Data availability

All data generated or analyzed during this study are included in this published article and its supplementary information files.

References

1. Sato, H. Tako-Tsubo-like left ventricular dysfunction due to multivessel coronary spasm. *Clin. Aspect Myocard. Injury: From Ischemia Heart Failure*. (1990).
2. Scally, C. et al. Persistent long-term structural, functional, and metabolic changes after stress-induced (takotsubo) cardiomyopathy. *Circulation* **137**, 1039–1048 (2018).
3. Templin, C. et al. Clinical features and outcomes of Takotsubo (stress) cardiomyopathy. *New Engl. J. Med.* **373**, 929–938 (2015).
4. Ghadri, J. R. et al. Long-term prognosis of patients with Takotsubo syndrome. *J. Am. Coll. Cardiol.* **72**, 874–882 (2018).
5. Paur, H. et al. High levels of circulating epinephrine trigger apical cardiodepression in a β2-adrenergic receptor/Gi-dependent manner: A new model of takotsubo cardiomyopathy. *Circulation* **126**, 697–706 (2012).
6. Wright, P. T., Tranter, M. H., Morley-Smith, A. C. & Lyon, A. R. Pathophysiology of Takotsubo syndrome. *Circ. J.* **78**, 1550–1558 (2014).
7. Heubach, J. F., Ravens, U. & Kaumann, A. J. Epinephrine activates both Gs and Gi pathways, but norepinephrine activates only the Gs pathway through human 2-adrenoceptors overexpressed in mouse heart. *Mol. Pharmacol.* **65**, 1313–1322 (2004).
8. Land, S. et al. Computational modeling of Takotsubo cardiomyopathy: effect of spatially varying-adrenergic stimulation in the rat left ventricle. *AJP Heart Circ. Physiol.* **307**, H1487–H1496 (2014).
9. Nef, H. M. et al. Abnormalities in intracellular Ca^{2+} regulation contribute to the pathomechanism of Tako-Tsubo cardiomyopathy. *Eur. Heart J.* **30**, 2155–2164 (2009).
10. Nef, H. M., Möllmann, H., Akashi, Y. J. & Hamm, C. W. Mechanisms of stress (Takotsubo) cardiomyopathy. *Nat. Rev. Cardiol.* **7**, 187–193 (2010).
11. Akashi, Y. J., Nef, H. M. & Lyon, A. R. Epidemiology and pathophysiology of Takotsubo syndrome. *Nat. Rev. Cardiol.* **12**, 387–397 (2015).
12. Ito, K. & Sugihara, H. Assessment of Takotsubo cardiomyopathy (transient left ventricular apical. *Ann. Nucl. Med.* **19**, 435–445 (2005).
13. Sestini, S. et al. The natural history of takotsubo syndrome: a two-year follow-up study with myocardial sympathetic and perfusion G-SPECT imaging. *Eur. J. Nucl. Med. Mol. Imaging* **44**, 267–283 (2017).
14. Jacobson, A. F. et al. Myocardial iodine-123 meta-iodobenzylguanidine imaging and cardiac events in heart failure. Results of the prospective ADMIRE-HF (AdreView myocardial imaging for risk evaluation in heart failure) study. *J. Am. Coll. Cardiol.* **55**, 2212–2221 (2010).
15. Kioka, H. et al. Prediction of sudden death in patients with mild-to-moderate chronic heart failure by using cardiac iodine-123 metaiodobenzylguanidine imaging. *Heart* **93**, 1213–1218 (2007).
16. Wittstein, I. S. et al. Neurohumoral features of myocardial stunning due to sudden emotional stress. *N. Engl. J. Med.* **352**, 539–548 (2005).
17. Winogradow, J. et al. Tako-tsubo cardiomyopathy after administration of intravenous epinephrine during an anaphylactic reaction. *Int. J. Cardiol.* **147**, 309–311 (2011).
18. Analysis of published cases. Y-Hassan, S. Serotonin norepinephrine re-uptake inhibitor (SNRI)-, selective norepinephrine reuptake inhibitor (S-NRI)-, and exogenously administered norepinephrine-induced takotsubo syndrome. *Int. J. Cardiol.* **231**, 228–233 (2017).
19. Sachdeva, J., Dai, W. & Kloner, R. A. Functional and histological assessment of an experimental model of takotsubo's cardiomyopathy. *J. Am. Heart Assoc.* **3**, 1–14 (2014).
20. Shao, Y. et al. A mouse model reveals an important role for catecholamine-induced lipotoxicity in the pathogenesis of stress-induced cardiomyopathy. *Eur. J. Heart Fail.* **15**, 9–22 (2013).
21. Ning, B. et al. Luteolin-7-diglucuronide attenuates isoproterenol-induced myocardial injury and fibrosis in mice. *Acta Pharmacol. Sin.* **38**, 331–341 (2017).
22. Cao, X. et al. Estrogen resisted stress-induced cardiomyopathy through increasing the activity of β2AR-Gαs signal pathway in female rats. *Int. J. Cardiol.* **187**, 377–386 (2015).
23. Thoonen, R. et al. Functional brown adipose tissue limits cardiomyocyte injury and adverse remodeling in catecholamine-induced cardiomyopathy. *J. Mol. Cell Cardiol.* **84**, 202–211 (2015).
24. Willis, B. C. et al. Impaired oxidative metabolism and calcium mishandling underlie cardiac dysfunction in a rat model of post-acute isoproterenol-induced cardiomyopathy. *Am. J. Physiol. Heart Circ. Physiol.* **308**, H467–H477 (2015).
25. Lesizza, P. et al. Single-dose intracardiac injection of pro-regenerative microRNAs improves cardiac function after myocardial infarction. *Circ. Res.* **120**, 1298–1304 (2017).

26. Liu, L. et al. miR-208a as a biomarker of isoproterenol-induced cardiac injury in sod2+/− and C57BL/6J wild-type mice. *Toxicol. Pathol.* **42**, 1117–1129 (2014).
27. Shao, Y. et al. Novel rat model reveals important roles of β-adrenoreceptors in stress-induced cardiomyopathy. *Int. J. Cardiol.* **168**, 1943–1950 (2013).
28. Yokoyama, T. et al. Quantification of sympathetic hyperinnervation and denervation after myocardial infarction by three-dimensional assessment of the cardiac sympathetic network in cleared transparent murine hearts. *PLoS One* **12**, 1–13 (2017).
29. Miwa, K. et al. Axon guidance of sympathetic neurons to cardiomyocytes by glial cell line-derived neurotrophic factor (GDNF). *PLoS One* **8**, 1–11 (2013).
30. Ben-Zvi, A., Ben-Gigi, L., Klein, H. & Behar, O. Modulation of semaphorin3A activity by p75 neurotrophin receptor influences peripheral axon patterning. *J. Neurosci.* **27**, 13000–13011 (2007).
31. Ueyama, T. et al. Estrogen attenuates the emotional stress-induced cardiac responses in the animal model of Tako-Tsubo (Ampulla) cardiomyopathy. *J. Cardiovasc. Pharmacol.* **42**, 117–120 (2003).
32. Kam, K. W. L., Qi, J. S., Chen, M. & Wong, T. M. Estrogen reduces cardiac injury and expression of β1-adrenoceptor upon ischemic insult in the rat heart. *J. Pharmacol. Exp. Ther.* **309**, 8–15 (2004).
33. Moriya, M., Mori, H., Suzuki, N., Hazama, M. & Yano, K. Six-month follow-up of takotsubo cardiomyopathy with I-123-beta-metyl-iodophenyl pentadecanoic acid and I-123-meta-iodobenzyl-guanidine myocardial scintigraphy. *Intern. Med.* **41**, 829–833 (2002).
34. Verschure, D. O. et al. Tako-tsubo cardiomyopathy: How to understand possible pathophysiological mechanism and the role of 123I-MIBG imaging. *J. Nuclear Cardiol.* **21**, 730–738 (2014).
35. Kimura, K. et al. Cardiac sympathetic rejuvenation: A link between nerve function and cardiac hypertrophy. *Circ. Res.* **100**, 1755–1764 (2007).
36. Kimura, K. et al. Norepinephrine-induced nerve growth factor depletion causes cardiac sympathetic denervation in severe heart failure. *Auton. Neurosci.* **156**, 27–35 (2010).
37. Fukuda, K., Kanazawa, H., Aizawa, Y., Ardell, J. L. & Shivkumar, K. Cardiac innervation and sudden cardiac death. *Circ. Res.* **116**, 2005–2019 (2015).
38. Klusch, A. et al. Local NGF and GDNF levels modulate morphology and function of porcine DRG neurites Vitro. *PLoS One* **13**, 1–18 (2018).
39. Ieda, M. et al. Nerve growth factor is critical for cardiac sensory innervation and rescues neuropathy in diabetic hearts. *Circulation* **114**, 2351–2363 (2006).
40. Martinelli, P. M. et al. Rat heart GDNF: Effect of chemical sympathectomy. *Histochem. Cell Biol.* **118**, 337–343 (2002).
41. Ieda, M. et al. Sema3a maintains normal heart rhythm through sympathetic innervation patterning. *Nat. Med.* **13**, 604–612 (2007).
42. Kim, J. et al. Mechanical stretch induces myelin protein loss in oligodendrocytes by activating Erk1/2 in a calcium-dependent manner. *Glia* **68**, 2070–2085 (2020).
43. Li, Y. et al. A precise, controllable in vitro model for diffuse axonal injury through uniaxial stretch injury. *Front. Neurosci.* **13**, 1–11 (2019).
44. Costa, V. M. et al. Study of the potential toxicity of adrenaline to neurons, using the SH-SY5Y human cellular model. *Brazil. J. Pharm. Sci.* (2023).
45. Bachis, A., Cruz, M. I., Nosheny, R. L. & Italo, M. Chronic unpredictable stress promotes neuronal apoptosis in the cerebral cortex. *Neurosci. Lett.* **442**, 1–12 (2008).
46. Ieda, M. & Fukuda, K. New aspects for the treatment of cardiac diseases based on the diversity of functional controls on cardiac muscles: The regulatory mechanisms of cardiac innervation and their critical roles in cardiac performance. *J. Pharmacol. Sci.* **109**, 348–353 (2009).
47. Minardo, J. D. et al. Scintigraphic and electrophysiological evidence of canine myocardial sympathetic denervation and reinnervation produced by myocardial infarction or phenol application. *Circulation* **78**, 1008–1019 (1988).
48. Kasama, S. et al. Prognostic value of cardiac sympathetic nerve activity evaluated by [123I]m-iodobenzylguanidine imaging in patients with ST-segment elevation myocardial infarction. *Heart* **97**, 20–26 (2011).
49. Tamaki, S. et al. Cardiac iodine-123 metaiodobenzylguanidine imaging predicts sudden cardiac death independently of left ventricular ejection fraction in patients with chronic heart failure and left ventricular systolic dysfunction. *J. Am. Coll. Cardiol.* **53**, 426–435 (2009).
50. Oh, Y. S. et al. Spatial distribution of nerve sprouting after myocardial infarction in mice. *Heart Rhythm* **3**, 728–736 (2006).
51. Tainaka, K. et al. Whole-body imaging with single-cell resolution by tissue decolorization. *Cell* **159**, 911–924 (2014).
52. Susaki, E. A. et al. Advanced CUBIC protocols for whole-brain and whole-body clearing and imaging. *Nat. Protoc.* **10**, 1709–1727 (2015).
53. Kanda, Y. Investigation of the freely available easy-to-use software 'EZR' for medical statistics. *Bone Marrow Transplant.* **48**, 452–458 (2013).

Acknowledgements

Author contributions

K.M. and J.Lee designed the research, conducted the experiment, analyzed the data. K.M., J.Lee, and T.Y. wrote the manuscript. J.Li, H.Y., Y.K., K.H., and Y.S. reviewed the manuscript.

Funding

Declarations

Competing interests

The authors declare no competing interests.

Additional information

Supplementary Information The online version contains supplementary material available at https://doi.org/10.1038/s41598-025-94349-8.

Correspondence and requests for materials should be addressed to J.-K.L.

Reprints and permissions information is available at www.nature.com/reprints.

Publisher's note Springer Nature remains neutral with regard to jurisdictional claims in published maps and institutional affiliations.